Chemical Science

Accepted Manuscript

This article can be cited before page numbers have been issued, to do this please use: M. M. Guru, S. De, S. Dutta, D. Koley and B. Maji, *Chem. Sci.*, 2019, DOI: 10.1039/C9SC02492A.

ROYAL SOCIETY OF CHEMISTRY

rsc.li/chemical-science

View Article Online
DOI: 10.1039/C9SC02492A

ARTICLE

$B(C_6F_5)_3$-Catalyzed Dehydrogenative Cyclization of *N*-Tosylhydrazones and Anilines via a Lewis Adduct: A Combined Experimental and Computational Investigations†

Received 00th January 20xx,
Accepted 00th January 20xx

DOI: 10.1039/x0xx00000x

Murali Mohan Guru,‡ Sriman De,‡ Sayan Dutta, Debasis Koley* and Biplab Maji*

Tris(pentafluorophenyl)borane-catalyzed dehydrogenative-cyclization of *N*-tosylhydrazones with aromatic amines has been disclosed. This metal-free catalytic protocol is compatible with a range of functional groups to provide both symmetrical and unsymmetrical 3,4,5-triaryl-1,2,4-triazoles. Mechanistic experiments and density functional theory (DFT) studies suggest an initial Lewis adduct formation of *N*-tosylhydrazone with $B(C_6F_5)_3$ is followed by a sequential intermolecular amination of borane adduct with aniline, an intramolecular cyclization and a frustrated Lewis pair (FLP)-catalyzed dehydrogenation for the generation of substituted 1,2,4-triazoles.

Introduction

Tris(pentafluorophenyl)borane has recently emerged as a powerful Lewis acid catalyst.[1-3] The strong Lewis acidity[2-3] at the boron center allows establishing a wide range of organic transformations via C-B,[4-6] C-C,[7-10] C-N,[11, 12] C-O[13, 14] and C-Si[15-18] bond formations. Pioneered by Stephan and Erker, $B(C_6F_5)_3$ has gained popularity in the frustrated Lewis pair (FLP) chemistry which encompasses wide applications in organic reactions.[19-22] Indeed, numerous efforts have been devoted for the activation of alkenes and alkynes by FLPs for the formation of the cyclic scaffolds.[23-25] However, in many cases, the highly desirable catalytic reaction is obstructed by the initially formed stable borate adduct.[26-28] Consequently, $B(C_6F_5)_3$ catalyzed cyclization leading to the important heterocyclic scaffolds are rare.[29-32]

In this context, 1,2,4-triazoles are omnipresent heterocyclic motifs in numerous biologically active compounds[33, 34] and they also have wide applications in organic light emitting diodes,[35, 36] organic photovoltaic cells, electroluminescent devices,[37, 38] bi-stable resistive memory devices,[39] pesticides, and medicines.[40] Given their applications, a number of strategies have been implemented for the synthesis of 1,2,4-triazoles.[41-45] However, most of these methods are limited due to the use of a super-stoichiometric amount of reagents or oxidants, low chemo-selectivity, narrow functional group tolerance, multiple reaction steps, and the production of copious waste. And a catalytic metal- and oxidant-free, step-economical processes for an efficient synthesis of substituted 1,2,4-triazoles is in demand.

Lewis acid-base adducts are potential intermediates in a multitude of transformations.[46-48] Recently, Stephan and coworkers have reported that diphenyldiazomethane, obtained from corresponding *N*-tosylhydrazone in the presence of a base, readily forms adducts with $B(C_6F_5)_3$ (Scheme 1a).[49, 50] This has shifted the gear for metal-free N_2 activation closer to reality. Conversely, the direct interaction of *N*-tosylhydrazones with $B(C_6F_5)_3$ and its application in catalytic transformations have not been reported yet.

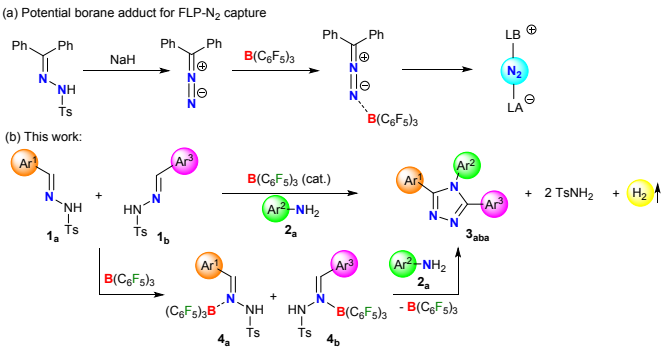

Scheme 1 Applications of borane adducts in main group chemistry.

On the other hand, the environmentally benign acceptorless catalytic dehydrogenations which are highly challenging even for transition-metal complexes[51, 52] are rare under metal-free conditions.[53-56] Very recently, we have presented a manganese-catalyzed acceptorless-dehydrogenative olefination of heteroarenes with primary alcohols.[57] Herein, we report $B(C_6F_5)_3$ catalyzed acceptorless-dehydrogenative-cyclization of *N*-tosylhydrazozes **1** and anilines **2** to triaryl-1,2,4-triazoles **3** via a borane adduct **4** followed by sequential C-N/N-N bond formations (Scheme 1b). Furthermore, extensive DFT calculations are performed not only to understand the mechanistic features of borane catalyzed triazole formation but also to assist future development of similar class of reaction.

Department of Chemical Sciences, Indian Institute of Science Education and Research Kolkata, Mohanpur-741246 (India). E-mail: koley@iiserkol.ac.in, bm@iiserkol.ac.in

†Electronic Supplementary Information (ESI) available: CCDC 1866759. For ESI and crystallographic data in CIF see DOI: 10.1039/x0xx00000x

‡These author contributed equally for this work.

Results and discussion

Initially, to check the reactivity of hydrazone **1a** with $B(C_6F_5)_3$, a stoichiometric reaction in benzene at room temperature was carried out. It leads to the formation of the Lewis adduct **4a** (δ ^{11}B –2.5 ppm) after 1h in 82% yield (Scheme 2). When **4a** was reacted with an aromatic amine **2a** at 80 °C in benzene, the 3,4,5-triaryl-1,2,4-triazole **3aaa** was formed in 85% NMR yield after 12 h along with an equimolar amount of $TsNH_2$ and $B(C_6F_5)_3$.

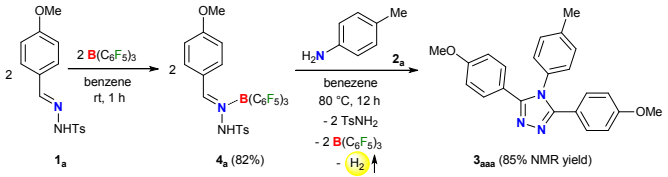

Scheme 2 Borane adduct of *N*-tosylhydrazone **1a** and its transformation.

As $B(C_6F_5)_3$ was finally released from the adduct **4a** after its reaction with the amine **2a**, it was posited that catalytic turnover should be possible under thermal condition. Interestingly, when the reaction was implemented with 5 mol % of $B(C_6F_5)_3$ at 80 °C the 1,2,4-triazole **3aaa** was obtained in 82% isolated yield along with 68% of $TsNH_2$ as a byproduct (Table 1, entry 1). While the increased catalyst loading did not significantly improve the yield (entry 2), a slight decrease in the product yield was observed with 3 mol% of $B(C_6F_5)_3$ (entry 3). The use of less Lewis acidic boranes such as BPh_3 was unproductive (entry 4). In addition, less hindered boranes like $BF_3{\cdot}OEt_2$ resulted in no detectable product formation (entry 5). Other Lewis acid catalysts like $Sc(OTf)_3$, $FeCl_3$ and $ZnCl_2$ were also not effective for this reaction (entry 6, Scheme S9 and S10 in ESI†).

Table 1 Optimization of $B(C_6F_5)_3$ catalyzed cyclization of the hydrazone **1a** with the anilines **2a**[a]

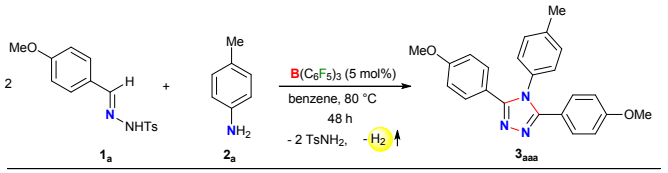

entry	deviation from above	yield (%)
1	none	82 (85)[b]
2	10 mol% $B(C_6F_5)_3$	83
3	3 mol% $B(C_6F_5)_3$	74
4	5 mol% $B(C_6H_5)_3$	n.r.
5	5 mol% $BF_3{\cdot}OEt_2$	n.r.
6	5 mol% $Sc(OTf)_3$ or $FeCl_3$ or $ZnCl_2$	n.r.

[a]Reaction Conditions: **1a** (0.5 mmol), **2a** (0.25 mmol), $B(C_6F_5)_3$ (5 mol%) in 2.0 mL benzene, Isolated yield. [b]NMR yield using 1,3,5-trimethoxybenzene as internal standard. n.r. = no reaction.

Next, the scope of this metal-free protocol was explored. A series of hydrazones **1** could be employed with various anilines **2** to afford symmetrical 3,4,5-triaryl-1,2,4-triazoles **3** in good to excellent yields (Table 2). The reaction of **1a** and **1b** with anilines **2a-f** bearing OMe-, Me-, H-, Cl- and Br- substituents at *para*- or *meta*-position of the aryl ring afforded the triazoles **3aab**-**3bbf** in 66-87% yields. Similarly, the hydrazones **1c-g** having substituents with different steric and electronic properties at the *ortho*-, *meta*-, and *para*-position on the aromatic rings could readily be cyclized with **2a** to produce **3cca**-**3gga** in 71-86% yields. The electronically biased aryl rings could be installed smoothly to get **3ccb**, **3hhb**, and **3iic** in 56-78% yields. Likewise, a thiophene- and fluorine-containing 1,2,4-triazoles **3eeh** and **3jjg** could be synthesized in 79% and 84% yields, respectively. Notably, an ester-group could also be tolerated under the reaction condition to accomplish **3kki** in 80% yield. On the other hand, substrate containing amide, nitro, olefin, primary alcohol, primary amino groups, *N*-tosylhydrazone of aliphatic aldehyde, and *N*-methanesulfonyl hydrazone were found to be unsuitable as either the starting materials were remain intact or a complex mixture of products were formed (Scheme S1-S5 in ESI†).

Table 2 $B(C_6F_5)_3$ catalyzed synthesis of symmetrical 1,2,4-triazoles[a]

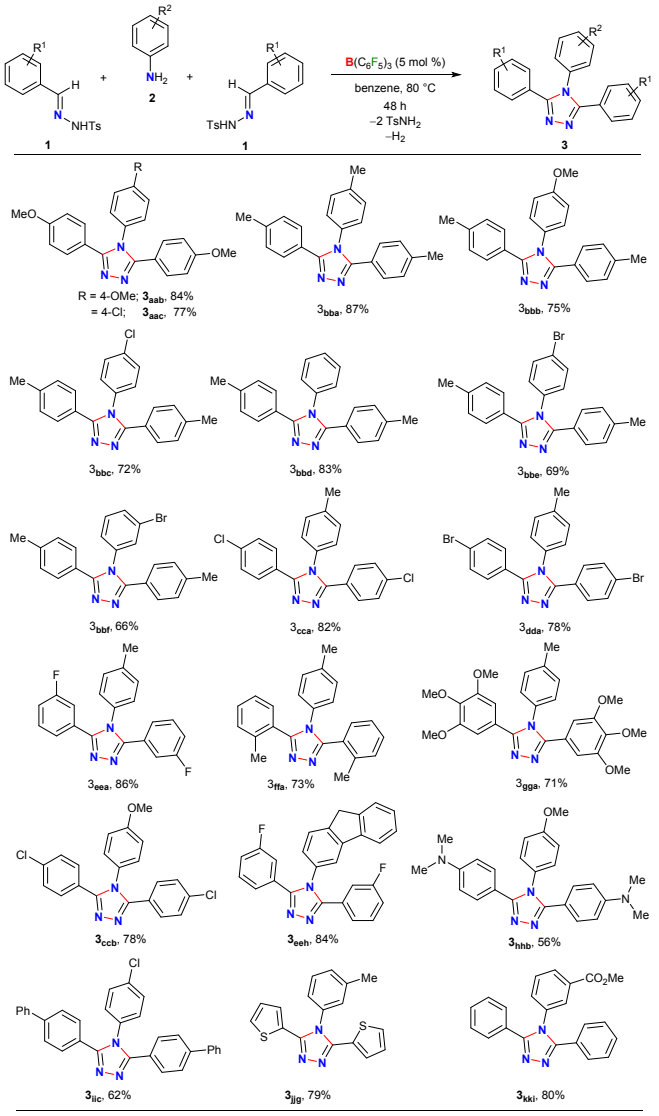

[a]Reaction condition: Table 1, entry 1. Yields of the analytically pure product.

To further demonstrate the applicability of our protocol, we examined the possibility of obtaining unsymmetrical 1,2,4-triazoles by employing two different hydrazones (Table 3). In fact, the synthesis of unsymmetrically substituted 1,2,4-triazoles are considered to be highly challenging and to best of

our knowledge, their single step synthesis from readily accessible starting material is less explored.[41-45] Gratifyingly, when **2a** was reacted with an equimolar mixture of **1a** and **1c** the unsymmetrical 1,2,4-triazole **3aca** was obtained as a major product in 77% yield and the symmetrical triazoles were only obtained in minor amounts. The products could be purified via column chromatography on silica-gel using ethyl acetate/hexane mixture as eluent. Similar reactivity and selectivity were also observed for the synthesis of **3ada** and **3aea**. Likewise, the biphenyl-, haloaromatic- and heteroaromatic-rings could be installed without any difficulties to give the triazoles **3aic**, **3aja**, **3akc**, **3bcb** and **3bdb** in 61-80% yields. Colorless crystals of **3aic**, grown from saturated benzene solution stored at room temperature, were suitable for single-crystal X-ray analysis and clearly confirmed the structure of the product (Figure S3 in ESI†).[58] It is noteworthy to mention that the reaction is highly chemoselective as the reactive carbomethoxy- and cyano-groups remain unaffected under the present reaction condition to provide **3aki** and **3alb** in 74% and 58% yields, respectively. The steric hindrance was found to exert a negligible influence on the reaction to give desired product **3bga** and **3bmf** in good yields.

Table 3 $B(C_6F_5)_3$ catalyzed synthesis of unsymmetrical 1,2,4-triazoles[a]

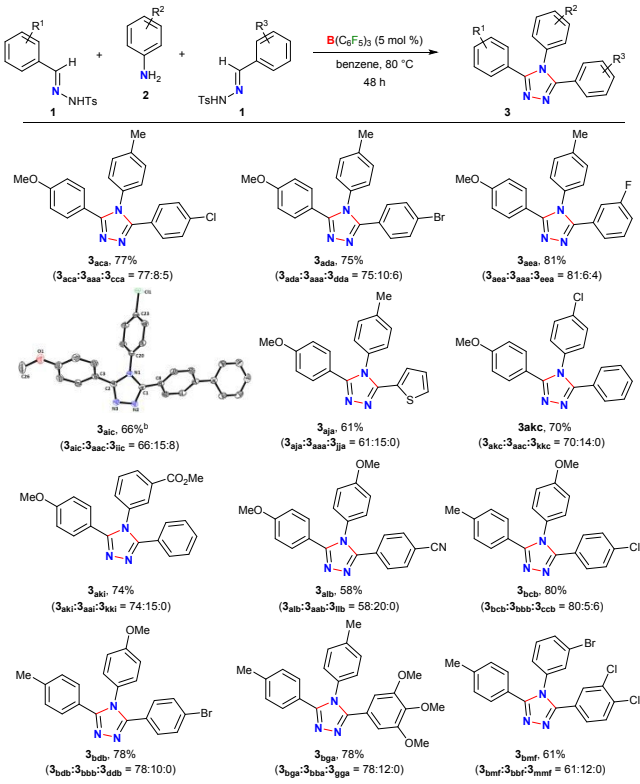

[a]Reaction condition: Table 1, entry 1 in 0.5 mmol scale. Yields of the analytically pure product. Selectivities are given in the parenthesis. [b]Thermal ellipsoids are shown at a 60% probability level. Ref [58].

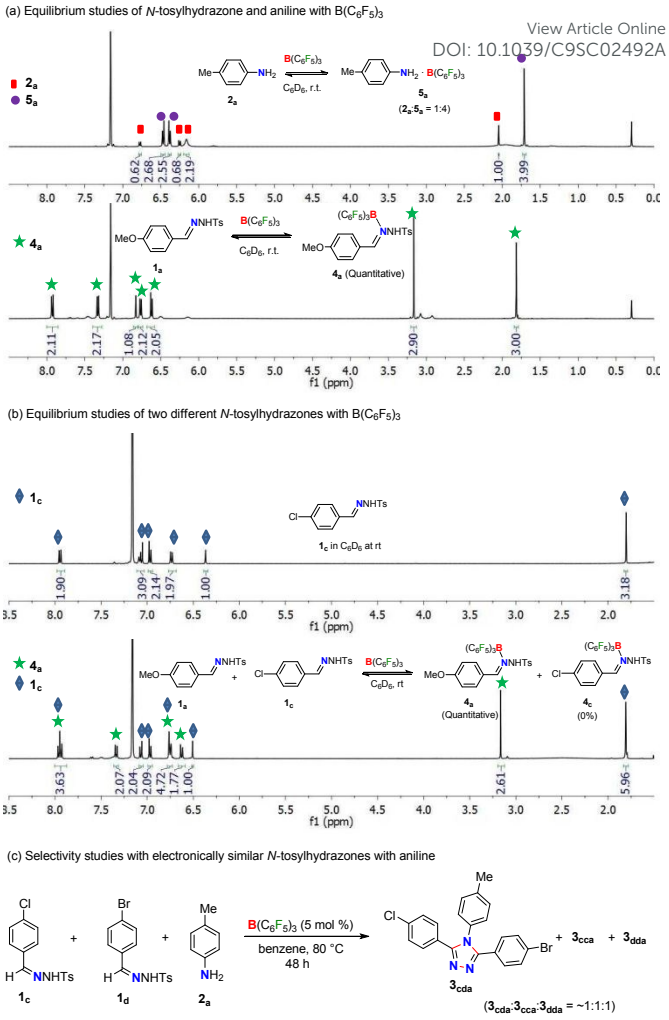

Scheme 3 Equilibrium and selectivity studies for 1,2,4-triazole formation.

In order to get insight into the reaction mechanism, initially several equilibrium studies with *N*-tosylhydrazones and anilines in the presence of Lewis acid were performed (Scheme 3). At the onset, the relative Lewis basicity of aniline and *N*-tosylhydrazone towards $B(C_6F_5)_3$ was analyzed (Scheme 3a). Thus, a stoichiometric reaction of **2a** and $B(C_6F_5)_3$ at room temperature in C_6D_6 the ratio of **2a** and **5a** ($B(C_6F_5)_3$ adduct of **2a**) was found to be 1:4 (**2a**:**5a** = 1:4). Similarly, the stoichiometric mixture of **1a** and $B(C_6F_5)_3$ in C_6D_6 at room temperature afforded quantitative formation of **4a** ($B(C_6F_5)_3$ adduct **1a**) where **1a**:**4a** = 0:100. This confirms the tendency *N*-tosylhydrazone **1** to form stronger Lewis acid-base adduct with $B(C_6F_5)_3$ in comparison to aniline **2**. Moreover, a competitive equilibrium study was performed with two electronically biased *N*-tosylhydrazones (**1a** vs **1c**) with $B(C_6F_5)_3$ (Scheme 3b). Accordingly, a stoichiometric (1:1) mixture of **1a** and **1c** was treated with 1 equivalent of $B(C_6F_5)_3$ in C_6D_6 at room temperature. This selectively afforded the Lewis acid-base adduct **4a** whereas **1c** remains unreacted (**4a**:**1c** = 1:1). Thus, *N*-tosylhydrazones having electron rich arenes will form strong Lewis acid-base adducts than hydrazones having electron deficient arenes. This is possibly a crucial factor for the selectivity observed during the

View Article Online
DOI: 10.1039/C9SC02492A

unsymmetrical 1,2,4-triazoles synthesis in Table 3. Along this direction, in fact, the reaction of aniline **2$_a$** with a mixture of **1$_c$** and **1$_d$** having electronically similar substituents (Cl and Br) on arenes in the presence of $B(C_6F_5)_3$ catalyst provided a mixture of two symmetrical and unsymmetrical 1,2,4-triazoles (Scheme 3c) as both the hydrazones have similar probabilities for the formation of the Lewis acid-base adducts with $B(C_6F_5)_3$. Thus, electronically biased hydrazones are the good candidates for better selectivity of unsymmetrical triazoles.

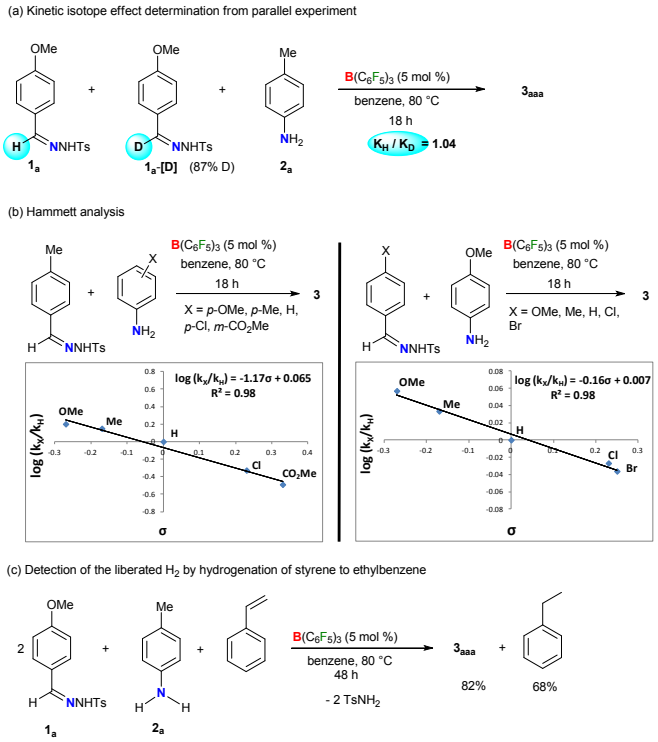

Scheme 4 Kinetic and mechanistic studies for the synthesis of 1,2,4-triazole.

In case of competitive equilibrium studies of two different anilines with $B(C_6F_5)_3$ a stoichiometric (1:1:1) mixture of **2$_a$**, **2$_c$** and $B(C_6F_5)_3$ in C_6D_6 at room temperature gave their corresponding Lewis acid-base adduct **5$_a$** and **5$_c$**, respectively in 8:1 ratio (Scheme S8 in ESI†). This indicates that highly basic anilines will form stronger adduct with $B(C_6F_5)_3$. It is also noteworthy to mention that the other Lewis acids like $Sc(OTf)_3$ and BPh_3 did not form any Lewis acid-base adducts with *N*-tosylhydrazones or anilines under the similar reaction conditions (Scheme S9 and S10 in ESI†).

In addition, the kinetic isotope effect (KIE) of 1.0 measured from a parallel reaction of **2$_a$** with **1$_a$** and its deuterated analogue **1$_a$-[D]** suggests that the breaking of imine C-H bond of **1$_a$** is not involved in the rate-determining step (Scheme 4a). Kinetic monitoring of the reaction suggests an exponential decay of both the reactants **1$_a$** and **2$_a$**, whereas sigmoidal increase of **3$_{aaa}$** was observed (Figure S1 in ESI†). The initial rate curve for triazole product formation possibly indicates that at the beginning the product formation is slower due to accumulation of reactive intermediates. Further kinetic studies revealed that the reaction is first order in the catalyst (Scheme S11 in ESI†) and aniline **2$_a$** (Scheme S12 in ESI†), and zero order in the *N*-tosylhydrazone **1$_a$** (Scheme S13 in ESI†). In addition, the electronic influence of the aryl-substituents on both the reactants was investigated by the Hammett correlation study (Scheme 4b). By varying different electronic groups on the aryl-ring of **2** a small $\rho = -1.17$ was obtained. This plausibly indicates a weak resonance interaction involving a positive-charge at the N center of aniline in the rate-determining-step. On the other hand, a negligible substituents effect ($\rho = -0.16$) was determined for *N*-tosylhydrazones. Meanwhile, the evolution of H_2 gas as a byproduct was confirmed by the transfer hydrogenation[59,60] of styrene under the reaction conditions (Scheme 4c). A 2:1:1 mixture of **1$_a$**, **2$_a$** and styrene in the presence of $B(C_6F_5)_3$ catalyst afforded 82% of **3$_{aaa}$** along with 68% of ethylbenzene (Scheme 4c). Moreover, we performed a number of control experiments using amidines, azines, and imines as possible reaction intermediates albeit none of them proceeded to give 1,2,4-triazoles (Scheme S14-S16 in ESI†).

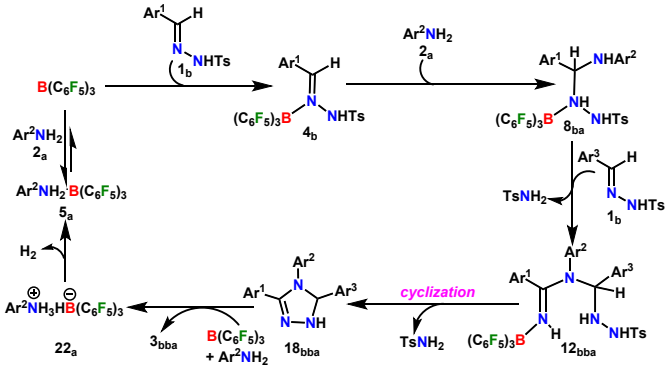

Scheme 5 Plausible reaction mechanism.

A plausible mechanism is proposed on the basis of the above experimental observations and previous literature reports (Scheme 5).[54,55] To the best of our knowledge DFT calculations of N-N cyclization leading to 1,2,4 triazole fragment is obscure. Based on the proposed mechanism of the $B(C_6F_5)_3$-catalyzed acceptorless-dehydrogenative-cyclization of *N*-tosylhydrazones with anilines (Scheme 5), we have performed DFT calculations to investigate the detailed reaction mechanism and to gain insight into the driving force for the formation of 1,2,4-triazole moiety **3$_{bba}$**. Additionally, the calculations seek to address some pertinent questions for the studied system: a) Specific role of $B(C_6F_5)_3$ in the reaction, b) rate-limiting-step in the reaction, and c) product distribution for unsymmetrical coupling.

The reaction is initiated with the coordination of $B(C_6F_5)_3$ to the *sp*^{2} nitrogen (N^1) in *N*-tosylhydrazone (**1$_b$**) which results in the formation of an isoenergetic encounter complex **4$_b^p$** (Scheme 6). The approach of the nucleophilic N^1 center in **1$_b$** towards the electron-deficient B center in $B(C_6F_5)_3$ furnishes the slightly more stable Lewis adduct **4$_b$** *via* transition state **[4^p-4]$_b^‡$** with an activation barrier of 10.9 kcal mol^{-1}. Despite the fact that the N^2 center in **1$_b$** is significantly electron-rich (-0.646 *e*) compared to the N^1 center (-0.242 *e*), as obtained by the natural population analysis (NPA), $B(C_6F_5)_3$ gets coordinated to the N^1 center. This is attributed to the fact that the lone pair orbital located on the N^1 atom (HOMO-4) is significantly destabilized compared to the one on N^2 atom (HOMO-5) by 0.4 eV (Fig. S100 in ESI†).

View Article Online
DOI: 10.1039/C9SC02492A

Furthermore, coordination at N^2 center resulted to adduct **4b´**, which is unstable than $\mathbf{4_b^p}$ by 2.4 kcal mol^{-1} (Scheme S17 in ESI†).

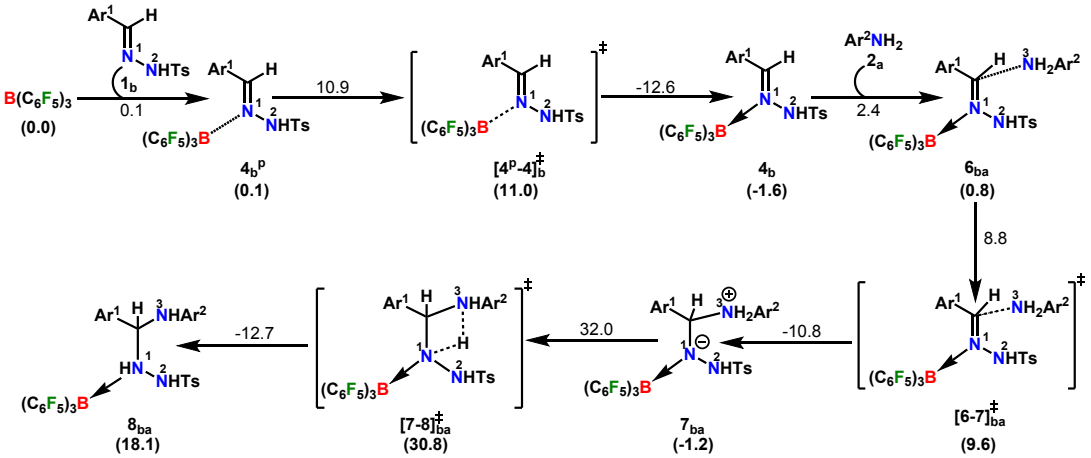

Scheme 6 *Part I*: Reaction pathway for the formation of the intermediate $\mathbf{8_{ba}}$. The energy values above the arrows denote the Gibbs free energy changes (ΔG_L^S) of the individual steps. The values in parentheses are the relative ΔG_L^S energies w.r.t the starting structures. All energy terms are in kcal mol^{-1}.

To cast light on the origin of the activation barrier and the bonding scenario in $\mathbf{[4^p\text{-}4]_b^{\ddagger}}$, EDA-NOCV (energy decomposition analysis-natural orbital for chemical valence) analysis was performed, considering $\mathbf{1_b}$ and $B(C_6F_5)_3$ as interacting fragments (Table S4 in ESI†). Examination of the individual energy terms of the EDA reveals that the B–N^1 bond has higher electrostatic character (ΔE_{elstat}: 39.8%) than the covalent nature (ΔE_{orb}: 33.5%). Importantly, the major contribution to the total covalent interaction (ΔE_{orb}) originates from the donation of the lone pair on the N^1 center in $\mathbf{1_b}$ to the vacant $2p_z$ orbital of boron in $B(C_6F_5)_3$ fragment (Fig. S101 in ESI†). We have calculated the associated eigenvalue of 0.49 *e* quantifying the amount of charge flow from donor → acceptor fragments. Additionally, the $B(C_6F_5)_3$ fragment has the predominant contribution to the destabilizing distortion energy (ΔE_{dis}). Calculated electron density [ρ(r)] of 0.112 at the (3, −1) bond critical point (BCP) of B–N^1 bond in $\mathbf{4_b}$ along with the respective Laplacian of +0.192 [$\nabla^2\rho$(r)], suggests a donor- acceptor type interaction.[61, 62] Thereafter, the coordination of the substituted aniline ($\mathbf{2_a}$) to $\mathbf{4_b}$ affords the intermediate $\mathbf{6_{ba}}$ which finally leads to a slightly more stable Zwitterionic complex $\mathbf{7_{ba}}$ accompanying moderately low energy barrier of 8.8 kcal mol^{-1}. The imaginary mode in $\mathbf{[6\text{-}7]_{ba}^{\ddagger}}$ portrays the formation of the C–N^3 bond (1.849 Å) along with concomitant elongation of C–N^1 bond (1.383 Å). It is worthwhile to mention that HOMO in $\mathbf{7_{ba}}$ represents the lone pair orbital located on the N^1 atom (Fig. S100 in ESI†). The subsequent proton transfer from N^3 to N^1 center in $\mathbf{7_{ba}}$ furnishes significantly less stable intermediate $\mathbf{8_{ba}}$ via a four-membered transition state $\mathbf{[7\text{-}8]_{ba}^{\ddagger}}$ (Scheme 6, Fig. 1a). The step $\mathbf{7_{ba}}$ → $\mathbf{8_{ba}}$, involving proton migration requires an activation barrier of 32.0 kcal mol^{-1} and thus becomes the rate-limiting-step for the overall transformation.[63] Indeed, this is supported by the experimental rate curve with slower rate at the beginning of the reaction (*vide supra*, Fig. S1 in ESI†). The single imaginary mode in $\mathbf{[7\text{-}8]_{ba}^{\ddagger}}$ depicts the synchronous breaking of N^3–H (1.296 Å) and formation of N^1–H (1.353 Å) bonds. In $\mathbf{[7\text{-}8]_{ba}^{\ddagger}}$, the B–$N^1$ bond gets significantly elongated (1.602/1.676 Å in $\mathbf{7_{ba}}$/$\mathbf{[7\text{-}8]_{ba}^{\ddagger}}$) and this weakening of the donor-acceptor bond is captured in the reduced NPA charge on the B center (+0.467/+0.488 e in $\mathbf{7_{ba}}$/$\mathbf{[7\text{-}8]_{ba}^{\ddagger}}$). It should be noted that both aniline and $TsNH_2$ assisted alternative intermolecular proton transfer between the two nitrogen (N^3 → N^1) are less favorable than the intramolecular path reported in Scheme 6 (Scheme S18a,b in ESI†).

From here on coupling of a second *N*-Tosylhydrazone unit is required for the progress of the reaction. This is accomplished through an initial proton transfer from C center in $\mathbf{8_{ba}}$ to the N^4 in $\mathbf{1_b}$. Such proton abstraction from tertiary C atom is manifested with N^1–N^2 bond elongation. This intermolecular proton transfer is clearly favorable (-17.5 kcal mol^{-1}), creating charged species $\mathbf{1_b^+}$ and $\mathbf{9_{ba}}$ respectively (Scheme 7). Whereas coordination of $\mathbf{1_b}$ instead of proton transfer is highly unfavorable (refer Scheme S18c in ESI†). In accordance with the experimental findings, KIE measurements suggest the non-involvement of imine C–H bond cleavage in the rate-determining-step (Scheme 4a). Though obvious, but important to note that hydrogen abstraction from electronegative N centers in $\mathbf{8_{ba}}$ is undoubtably difficult leading to highly unstable intermediates (Scheme S18d in ESI†). Close inspection of structural parameters in $\mathbf{9_{ba}}$ indicates considerable elongation, rather dissociation of the N^1–N^2 bond (1.450 Å/2.987 Å = $\mathbf{8_{ba}}$/$\mathbf{9_{ba}}$) and generation of partial double bond character in the C–N^1 bond (1.568 Å/1.323 Å = $\mathbf{8_{ba}}$/$\mathbf{9_{ba}}$) The N^2 center of -NHTS unit in $\mathbf{9_{ba}}$ shows significant hydrogen bonding interaction with the H^2 atom connected to the N^3 center, as evidenced by the N^3–H^2 (1.088 Å) and N^2–H^2 (1.622 Å) bond lengths. The dissociation of $TsNH_2$ fragment is quite evident from $\mathbf{10_{ba}}$ with shorter N^2–H^2 distance (1.057 Å) and further elongated N^1–N^2 distance (3.634 Å). Complete removal of $TsNH_2$ will generate a highly nucleophilic N^3

View Article Online
DOI: 10.1039/C9SC02492A

center in $\mathbf{11_{ba}}$ which will immediately coordinate with the preformed cationic intermediate $\mathbf{1_b^+}$ to generate substantially stable $\mathbf{12_{bba}}$ (Scheme 7). The coupling of two oppositely charged species is further facilitated by the exothermicity of the C–N^3 bond formation.

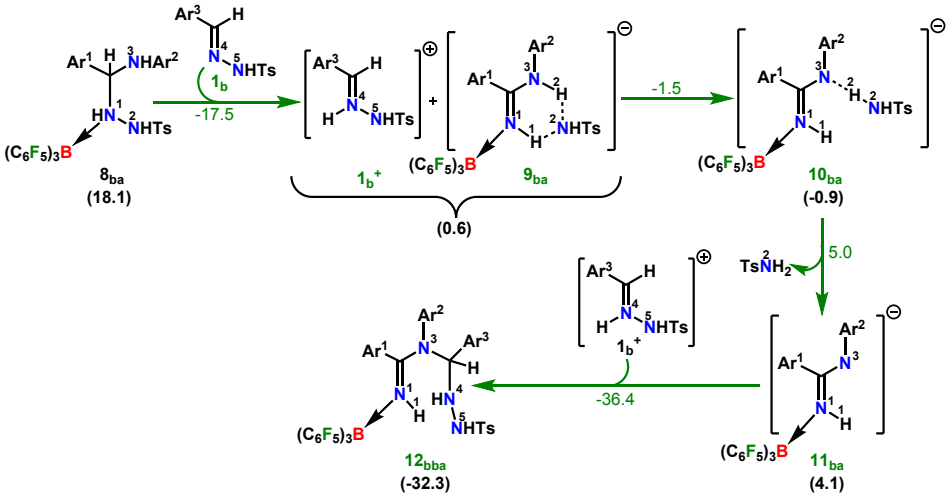

Scheme 7 *Part II*: Reaction pathway for the formation of intermediate $\mathbf{12_{bba}}$. For other information refer caption in Scheme 6.

From $\mathbf{12_{bba}}$ the cyclization step is necessary to generate the triazole product $\mathbf{3_{bba}}$ (Scheme 5). Under these circumstances, it might be conceivable that liberation of second $TsNH_2$ unit will facilitate the N^1–N^4 bond formation. Thus, protonation at the N^5 center is necessary, similar to the preceding step $\mathbf{8_{ba}} \rightarrow \mathbf{1_b^+} + \mathbf{9_{ba}}$ in *Part II* (Scheme 7). Unlike from $\mathbf{8_{ba}}$, possibility for C–H abstraction in $\mathbf{12_{bba}}$ either as proton or hydride transfer is unfeasible (refer Scheme S18e in ESI†). However, formation of cationic species $\mathbf{13_{bba}}$ after protonation along with anionic $\mathbf{9_{ba}}$ generation is possible, but less exothermic than the previous transfer ($\mathbf{8_{ba}} \rightarrow \mathbf{1_b^+} + \mathbf{9_{ba}}$; Schemes 7, 8). Unfortunately, addition of proton to any other electronegative centers resulted in either high energy intermediates or reaction dead ends (refer Scheme S18f in ESI†). In order to enhance the nucleophilicity at N^1 center, $B(C_6F_5)_3$ was decoordinated in presence of aryl amine ($\mathbf{2_a}$) to generate notably unstable $\mathbf{14_{bba}}$ (Scheme 8). Subsequent rearrangement to isomeric $\mathbf{15_{bba}}$ provides adequate structural disposition for facile cyclization to proceed. We have explored numerous possibilities for N^1-N^4 bond formation. However, none of them gave promising alternatives instead the activation barriers are too high or transition states could not be optimized after numerous attempts (Scheme S18g in ESI†). The cyclization step involving transition state $\mathbf{[15\text{-}16]_{bba}}^{\ddagger}$ requires an activation barrier of 15.8 kcal mol^{-1} and it witness a progressive removal of $TsNH_2$ unit.

As expected, the transition vector in $\mathbf{[15\text{-}16]_{bba}}^{\ddagger}$ animates weakening of the N^4–N^5 bond (1.794 Å) with concomitant formation of N^1–N^4 bond (2.192 Å). Complete removal of $TsNH_2$ affords the saturated triazole intermediate $\mathbf{17_{bba}}$, which is 35.6 kcal mol^{-1} stable than $\mathbf{15_{bba}}$. Subsequent deprotonation at N^1 center by $\mathbf{1_b}$ will generate significantly less stable intermediate $\mathbf{18_{bba}}$.[64] This step is facile with activation barrier of only 1.6 kcal/mol (Scheme S19 in ESI†). The protonated form $\mathbf{1_b^+}$ generated can have two fates: it may either participate in the preceding steps reported in *Part II* (Scheme 7) or can undergo an endergonic exchange of proton to a free amine ($\mathbf{2_a} + \mathbf{1_b^+} \rightarrow \mathbf{2_a^+} + \mathbf{1_b}$; 4.8 kcal mol^{-1}). Generally, intermediates formed after coupling of second *N*-tosylhydrazone moiety is highly stable as compared to the starting structures and the driving force for the subsequent reactions is the increasing exergonicity towards product formation (refer Fig. 1b). This statement gets support from the high-resolution-mass-spectrometry studies which clearly detect the similar skeleton as that of $\mathbf{18_{bba}}$ (Fig. S2 in ESI†). In order to address the positional effect of $B(C_6F_5)_3$ in the cyclization step, we calculated two isomers where it coordinates to other N centers (N^4 and N^5) in $\mathbf{12_{bba}}$. The resulting intermediates $\mathbf{35_{bba}}$ and $\mathbf{36_{bba}}$ are unstable and did not provide a low energy route to the cyclization step (Scheme S18h in ESI†). Furthermore, in absence of $B(C_6F_5)_3$ the cyclization step leading to $\mathbf{18_{bba}}$ encounters high transition barrier (38.2 kcal mol^{-1}; Scheme S18i in ESI†) and thus underscores the significance of $B(C_6F_5)_3$ in this current transformation.

In the next step, $\mathbf{18_{bba}}$ undergoes dehydrogenative aromatization[54, 55] to furnish triazole $\mathbf{3_{bba}}$ and an ion pair $\mathbf{22_a}$ through $B(C_6F_5)_3$ mediated hydride abstraction ($\mathbf{19_{bba}} \rightarrow \mathbf{20_{bba}}$) followed by proton abstraction involving substituted aniline ($\mathbf{21_{bba}} \rightarrow \mathbf{3_{bba}} + \mathbf{22_a}$; Scheme 9). We have calculated the intrinsic activation barriers of 13.1 and 21.7 kcal mol^{-1} for the hydride and proton abstraction steps, respectively. Thereafter, two hydrogen atoms in the ion pair $\mathbf{22_a}$ produce H_2 molecule via the four-membered transition state $\mathbf{[22\text{-}5]_a}^{\ddagger}$ (Scheme 9, Fig. 1b). Liberation of H_2 along with the formation of frustrated Lewis acid-base pair (FLP) adduct $\mathbf{5_a}$ is facile with barrier of only 11.3 kcal mol^{-1} (Scheme 9). Evolution of H_2 was also confirmed by the transfer hydrogenation of styrene (*vide supra,* Scheme 4c). Finally, maintaining an endoergic equilibrium, the FLP adduct regenerates $B(C_6F_5)_3$ and substrate $\mathbf{2_a}$.[65] In sum, the computational results do have

concurrence with the experimental findings, particularly in understanding the dual role of $B(C_6F_5)_3$ in activating the *N*-tosylhydrazone towards nucleophilic attack and acceptor-less liberation of H_2 with formation of FLP (Scheme 9). Additionally, the rate determining step involving the intramolecular proton transfer ($\mathbf{7_{ba}} \rightarrow \mathbf{8_{ba}}$; $\Delta^{\ddagger}G^{S}$ = 32.0 kcal mol^{-1}) can be surmounted under the reaction temperature of 80 °C.[66] Optimized geometries of the transition states with selected geometrical parameters along with the energy profiles are collected in Fig. 1.

View Article Online
DOI: 10.1039/C9SC02402A

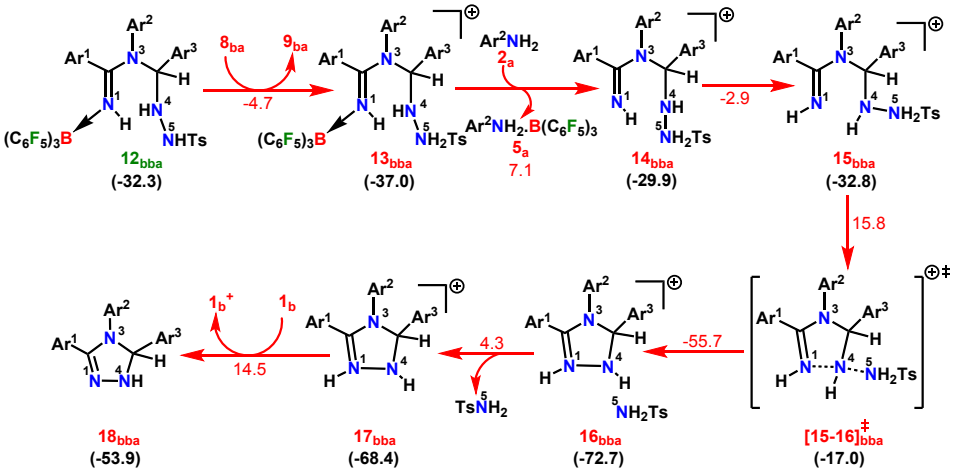

Scheme 8 *Part III*: Reaction pathway for the formation of intermediate $\mathbf{18_{bba}}$. For other information refer caption in Scheme 6.

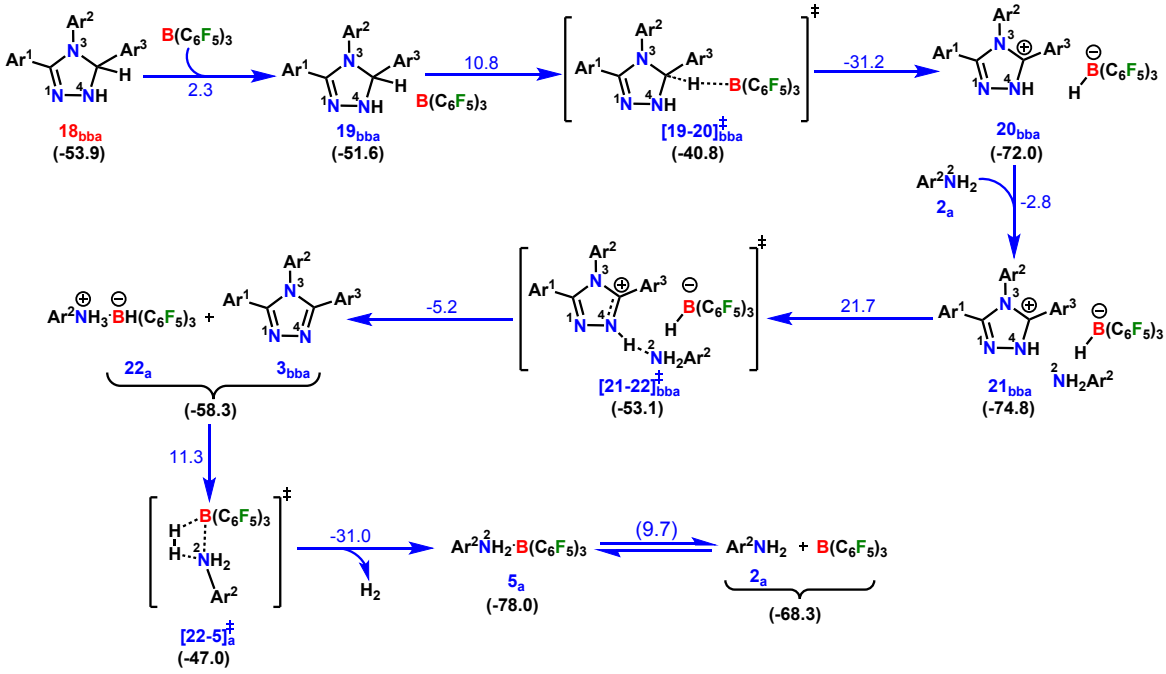

Scheme 9 *Part IV*: Reaction pathway for the formation of desired product 1,2,4-triazole complex ($\mathbf{3_{bba}}$) and hydrogen evolution step. For other information refer caption in Scheme 6

View Article Online
DOI: 10.1039/C9SC02492A

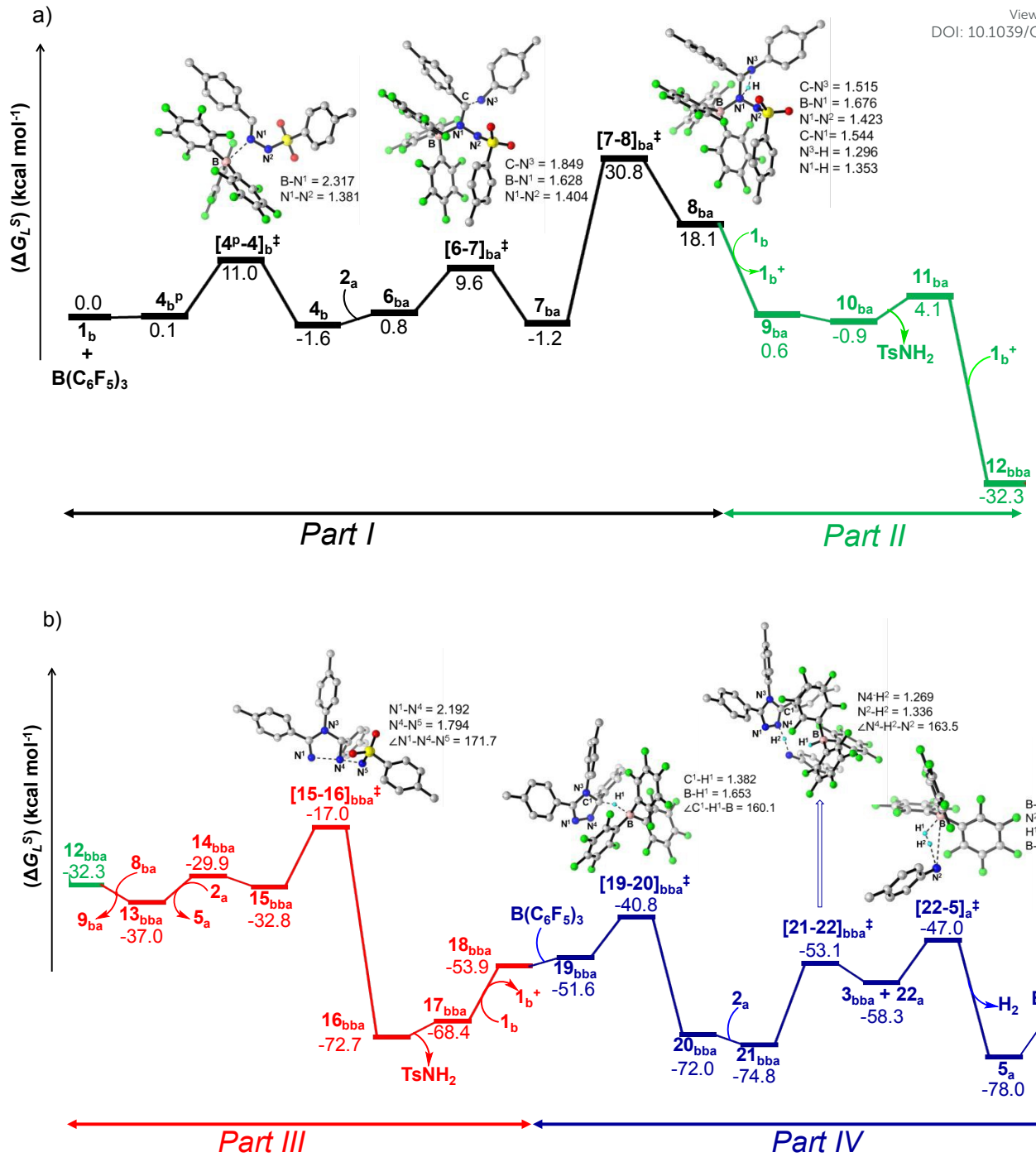

Fig. 1. Energy profile and 3D figures of optimized transition states with selected geometrical parameters for 1,2,4-triazole product ($\mathbf{3}_{bba}$) formation at B3LYP-D3/TZVP//B3LYP/SVP level. The black, green, red and blue colored pathways represent sections a) *Part I*, *Part II* and b) *Part III*, *Part IV*, respectively (refer Schemes 6-9). Bond distances are in angstroms (Å) and bond angles are in degrees (°).

For unsymmetrical Systems:

Equimolar mixture of $\mathbf{1}_a$ and $\mathbf{1}_c$ in presence of $\mathbf{2}_a$ afforded the unsymmetrical triazole $\mathbf{3}_{aca}$ as the major product (77%) than the symmetrical counterpart (*vide supra*; Table 3). To provide reasonable justification for this observation we decided to compare the relative propensity of Lewis acid-base adduct formation of *N*-tosylhydrazones $\mathbf{1}_a$ and $\mathbf{1}_c$ with $B(C_6F_5)_3$ ($B(C_6F_5)_3 \rightarrow \mathbf{4}_{a/c}{}^p \rightarrow \mathbf{4}_{a/c}$). As expected, the formation of $\mathbf{4}_a$ is more facile than $\mathbf{4}_c$ by ca 3.0 kcal mol^{-1} (Fig. S102 in ESI†). This is in accordance with the experimentally observed equilibrium ratio in Scheme 3b. Eventually the activation barrier for $B(C_6F_5)_3$ coordination is favorable for the -OMe substituent by 3.6 kcal mol^{-1} ($\Delta\Delta G_L^{S\ddagger}$; Fig. S102 in ESI†). What is more interesting is that the overall energy span for *Part I* is substantially higher for -Cl substituent than -OMe (42.5 kcal mol^{-1} vs. 33.3 kcal mol^{-1}), clearly indicating the

preference for $\mathbf{1_a}$ to undergo $B(C_6F_5)_3$ assisted intra-molecular proton transfer to be facile. Therefore, when $\mathbf{8_{aa}}$ will couple with another hydrazone unit, the preferred choice will be the chloro-substituted analogue $\mathbf{1_c}$ as most of the $\mathbf{1_a}$ will be available in the adduct form $\mathbf{4_a}$. Combination of $\mathbf{8_{aa}}$ with $\mathbf{1_c}$ will lead directly to $\mathbf{12_{aca}}$ in a favorable fashion with exothermicity of -50.6 kcal mol^{-1} (Figure S103 in ESI†). From $\mathbf{12_{aca}}$, generation of $\mathbf{16_{aca}}$ requires a barrier of 20.4 kcal mol^{-1} almost similar to the value obtained in the previous case (20.0 kcal mol^{-1}: $\mathbf{12_{bba}} \rightarrow \mathbf{16_{bba}}$: Fig. 1b). This barrier is 1.1 kcal mol^{-1} lower than the symmetrical case (Fig. S103 in ESI†) further supporting the preference for unsymmetrical triazole ($\mathbf{3_{aca}}$) formation (Fig. S103 in ESI†). After the formation of triazole ring in $\mathbf{16_{aca}}$, which is -71.5 kcal mol^{-1} stable than the starting materials, the subsequent $B(C_6F_5)_3$ assisted dehydrogenation will follow an analogous mechanism as outlined before (Scheme 9; Fig. 1b).[67]

Conclusions

In summary, we have demonstrated $B(C_6F_5)_3$ catalyzed metal-free, one-pot, dehydrogenative-cyclization of hydrazones with anilines to furnish both symmetrical and unsymmetrical 3,4,5-triaryl-1,2,4-triazoles. The isolation of the *N*-tosylhydrazone-borane adduct is also reported for the first time. The mechanistic experiments and DFT calculations suggest that the $B(C_6F_5)_3$ catalyst serves a dual role; the activation of the hydrazone for the nucleophilic attack and the formation of an FLP for dehydrogenation. Calculations also reveal that the rate-determining step involves intra-molecular hydrogen transfer between the N-centers after aniline gets bonded to the *N*-Tosylhydrazone unit. The chemo-selective, step-economical, oxidant-free and mild reaction protocol could give a prospective luminescence for the increasing focus on main-group catalyzed chemical transformation to circumvent transition metals.

Computational Methods

All computations are performed using Gaussian 09[68] and ADF 2018.103[69] quantum codes. Geometry optimizations of the saddle points without any symmetry constraints are carried out using B3LYP hybrid functional[70] in conjunction with SVP basis set[71] in the Gaussian 09 program package. Harmonic force constants are computed at the optimized geometries to characterize the nature of the stationary points as minima (N_{img} = 0) or transition states (N_{img} = 1). Transition states are located by using the linear synchronous transit (LST)[72] scan method in which the reaction coordinate was kept fixed at different distances while all other degrees of freedom are relaxed. After the linear transit search, the transition states are optimized by using the default Berny algorithm implemented in the Gaussian 09 code. All transition states are validated by intrinsic reaction coordinate (IRC) calculations. In addition, single point calculations were performed on the B3LYP/SVP optimized structures using dispersion corrected hybrid functional B3LYP-D3[73] in conjunction with a large basis set (triple-ζ quality split valence plus polarization TZVP).[74] The effect of solvation (benzene, dielectric constant ε = 2.27) was assessed by a self-consistent reaction field (SCRF) approach, using the conductor-like polarizable continuum model (CPCM).[75] Tight wave function convergence criteria and an "ultrafine" (99 950) grid was used for the single point calculations. Natural bond orbital (NBO)[76] analysis was performed at the B3LYP-D3/TZVP//B3LYP/SVP level using the NBO Version 3.1 program. QTAIM (Quantum Theory of Atoms in Molecules) calculations are also performed to characterize the electron distribution around some selected bonds in the chemical species applying Bader's AIM (atoms-in-molecule) theory.[77] Furthermore, to gain insight into the bonding scenario in transition state $\mathbf{[4^p\text{-}4]_b^{\ddagger}}$, EDA (energy decomposition analysis) calculations in conjunction with the NOCV (natural orbital for chemical valence)[78] method are undertaken using the ADF 2018.103 package. Implementation and application of the EDA method, which was originally developed by Morokuma[79] and later modified by Ziegler and Rauk,[80] can be found elsewhere.[81-85] Figures reported in the manuscript are generated using ChemDraw Ultra 12.0 and CYLview[86] visualization softwares.

Conflicts of interest

There are no conflicts to declare.

Acknowledgements

We thank IISER Kolkata (Start-up grant) for financial support. M.M.G. thanks SERB (PDF/2017/000028) for the NPDF fellowship. S. De and S. Dutta thank UGC and CSIR, respectively for senior research fellowships. D.K. acknowledges the funding from bilateral DST-DFG (INT/FRG/DFG/P-05/2017) scheme and IISER Kolkata for computational facility. The authors thank Dr. S. Lakhdar (CNRS–ENSI Caen), and Prof. Dr. H. Mayr (LMU Munich) for helpful discussions.

Notes and references

1 W. E. Piers and T. Chivers, *Chem. Soc. Rev.*, 1997, **26**, 345-354.
2 (a) K. Ishihara, N. Hananki, H. Yamamoto, *Synlett* 1993, 577–579; (b) K. Ishihara, M. Funahashi, M. Miyata, H. Yamamoto, *Synlett* 1994, 963–964; (c) K. Ishihara, N. Hanaki, M. Funahashi, M. Miyata, H. Yamamoto, *Bull. Chem. Soc. Jpn.* 1995, **68**, 1721–1730; (d) G. Erker, *Dalton Trans.*, 2005, 1883-1890.
3 J. R. Lawson and R. L. Melen, *Inorg. Chem.*, 2017, **56**, 8627-8643.
4 R. L. Melen, L. C. Wilkins, B. M. Kariuki, H. Wadepohl, L. H. Gade, A. S. K. Hashmi, D. W. Stephan and M. M. Hansmann, *Organometallics*, 2015, **34**, 4127-4137.
5 G. Kehr and G. Erker, *Chem. Sci.*, 2016, **7**, 56-65.
6 J. S. McGough, S. M. Butler, I. A. Cade and M. J. Ingleson, *Chem. Sci.*, 2016, **7**, 3384-3389.
7 S. Tamke, Z.-W. Qu, N. A. Sitte, U. Floerke, S. Grimme and J. Paradies, *Angew. Chem., Int. Ed.*, 2016, **55**, 4336-4339.

8 M. Shang, M. Cao, Q. Wang and M. Wasa, *Angew. Chem., Int. Ed.*, 2017, **56**, 13338-13341.
9 C. K. Hazra, J. Jeong, H. Kim, M.-H. Baik, S. Park and S. Chang, *Angew. Chem., Int. Ed.*, 2018, **57**, 2692-2696.
10 M. Shang, J. Z. Chan, M. Cao, Y. Chang, Q. Wang, B. Cook, S. Torker and M. Wasa, *J. Am. Chem. Soc.*, 2018, **140**, 10593-10601.
11 M. Shang, X. Wang, S. M. Koo, J. Youn, J. Z. Chan, W. Yao, B. T. Hastings and M. Wasa, *J. Am. Chem. Soc.*, 2017, **139**, 95-98.
12 Y. Hoshimoto, T. Kinoshita, S. Hazra, M. Ohashi and S. Ogoshi, *J. Am. Chem. Soc.*, 2018, **140**, 7292-7300.
13 D. J. Faizi, A. Issaian, A. J. Davis and S. A. Blum, *J. Am. Chem. Soc.*, 2016, **138**, 2126-2129.
14 H. H. San, S.-J. Wang, M. Jiang and X.-Y. Tang, *Org. Lett.*, 2018, **20**, 4672-4676.
15 C. K. Hazra, N. Gandhamsetty, S. Park and S. Chang, *Nat. Commun.*, 2016, **7**, 13431.
16 P. Smirnov and M. Oestreich, *Organometallics*, 2016, **35**, 2433-2434.
17 Y. Han, S. Zhang, J. He and Y. Zhang, *J. Am. Chem. Soc.*, 2017, **139**, 7399-7407.
18 Y. Ma, L. Zhang, Y. Luo, M. Nishiura and Z. Hou, *J. Am. Chem. Soc.*, 2017, **139**, 12434-12437.
19 K. Chernichenko, A. Madarasz, I. Papai, M. Nieger, M. Leskelae and T. Repo, *Nat. Chem.*, 2013, **5**, 718-723.
20 M.-A. Légaré, M.-A. Courtemanche, É. Rochette and F.-G. Fontaine, *Science*, 2015, **349**, 513-516.
21 D. W. Stephan and G. Erker, *Angew. Chem., Int. Ed.*, 2015, **54**, 6400-6441.
22 W. Meng, X. Feng and H. Du, *Acc. Chem. Res.*, 2018, **51**, 191-201.
23 A. Fukazawa, H. Yamada and S. Yamaguchi, *Angew. Chem., Int. Ed.*, 2008, **47**, 5582-5585.
24 C. M. Moemming, G. Kehr, B. Wibbeling, R. Froehlich, B. Schirmer, S. Grimme and G. Erker, *Angew. Chem., Int. Ed.*, 2010, **49**, 2414-2417.
25 X. Zhao and D. W. Stephan, *Chem. Sci.*, 2012, **3**, 2123-2132.
26 M. M. Hansmann, R. L. Melen, F. Rominger, A. S. K. Hashmi and D. W. Stephan, *Chem. Commun.*, 2014, **50**, 7243-7245.
27 M. M. Hansmann, R. L. Melen, M. Rudolph, F. Rominger, H. Wadepohl, D. W. Stephan and A. S. K. Hashmi, *J. Am. Chem. Soc.*, 2015, **137**, 15469-15477.
28 L. C. Wilkins, J. R. Lawson, P. Wieneke, F. Rominger, A. S. K. Hashmi, M. M. Hansmann and R. L. Melen, *Chem. - Eur. J.*, 2016, **22**, 14618-14624.
29 T. Mahdi and D. W. Stephan, *Chem. - Eur. J.*, 2015, **21**, 11134-11142.
30 V. Fasano, J. E. Radcliffe and M. J. Ingleson, *Organometallics*, 2017, **36**, 1623-1629.
31 Y. Soltani, L. C. Wilkins and R. L. Melen, *Angew. Chem., Int. Ed.*, 2017, **56**, 11995-11999.
32 K. Yuan and S. Wang, *Org. Lett.*, 2017, **19**, 1462-1465.
33 G. M. Brittenham, D. G. Nathan, N. F. Olivieri, M. J. Pippard and D. J. Weatherall, *Lancet*, 2003, **361**, 183-184.
34 R. Tokala, S. Bale, I. P. Janrao, A. Vennela, N. P. Kumar, K. R. Senwar, C. Godugu and N. Shankaraiah, *Bioorg. Med. Chem. Lett.*, 2018, **28**, 1919-1924.
35 Q. Zhang, B. Li, S. Huang, H. Nomura, H. Tanaka and C. Adachi, *Nat. Photonics*, 2014, **8**, 326-332.
36 W. Song, L. Shi, L. Gao, P. Hu, H. Mu, Z. Xia, J. Huang and J. Su, *ACS Appl. Mater. Interfaces*, 2018, **10**, 5714-5722.
37 *WO Pat.*, WO2006114377A1, 2006.
38 *US Pat.*, US9113536B2, 2015.
39 B. K. Barman, M. M. Guru, G. K. Panda, B. Maji and R. K. Vijayaraghavan, *Chem. Commun.*, 2019, **55**, 4643-4646.
40 Y. Naito, F. Akahoshi, S. Takeda, T. Okada, M. Kajii, H. Nishimura, M. Sugiura, C. Fukaya and Y. Kagitani, *J. Med. Chem.*, 1996, **39**, 3019-3029.
41 A. Moulin, M. Bibian, A.-L. Blayo, S. El Habnouni, J. Martinez and J.-A. Fehrentz, *Chem. Rev.*, 2010, **110**, 1809-1827.
42 S. Ueda and H. Nagasawa, *J. Am. Chem. Soc.*, 2009, **131**, 15080-15081.
43 S. T. Staben and N. Blaquiere, *Angew. Chem., Int. Ed.*, 2010, **49**, 325-328.
44 H. Wang, Y. Ren, K. Wang, Y. Man, Y. Xiang, N. Li and B. Tang, *Chem. Commun.*, 2017, **53**, 9644-9647.
45 Z. Ye, M. Ding, Y. Wu, Y. Li, W. Hua and F. Zhang, *Green Chem.*, 2018, **20**, 1732-1737.
46 C. Appelt, J. C. Slootweg, K. Lammertsma and W. Uhl, *Angew. Chem., Int. Ed.*, 2013, **52**, 4256-4259.
47 K. L. Bamford, L. E. Longobardi, L. Liu, S. Grimme and D. W. Stephan, *Dalton Trans.*, 2017, **46**, 5308-5319.
48 T. C. Johnstone, G. N. J. H. Wee and D. W. Stephan, *Angew. Chem., Int. Ed.*, 2018, **57**, 5881-5884.
49 C. Tang, Q. Liang, A. R. Jupp, T. C. Johnstone, R. C. Neu, D. Song, S. Grimme and D. W. Stephan, *Angew. Chem., Int. Ed.*, 2017, **56**, 16588-16592.
50 R. L. Melen, *Angew. Chem., Int. Ed.*, 2018, **57**, 880-882.
51 C. Gunanathan and D. Milstein, *Science*, 2013, **341**, 249.
52 R. H. Crabtree, *Chem. Rev.*, 2017, **117**, 9228-9246.
53 Z. Lu, L. Schweighauser, H. Hausmann and H. A. Wegner, *Angew. Chem., Int. Ed.*, 2015, **54**, 15556-15559.
54 (a) M. Kojima and M. Kanai, *Angew. Chem., Int. Ed.*, 2016, **55**, 12224-12227.
55 (a) A. F. G. Maier, S. Tussing, T. Schneider, U. Floerke, Z.-W. Qu, S. Grimme and J. Paradies, *Angew. Chem., Int. Ed.*, 2016, **55**, 12219-12223; (b) Z.-J. Cai, X.-M. Lu, Y. Zi, C. Yang, L.-J. Shen, J. Li, S.-Y. Wang and S.-J. Ji, *Org. Lett.* 2014, **16**, 5108-5111; (c) Z. Chen, Q. Yan, Z. Liu and Y. Zhang, *Chem. - Eur. J.* 2014, **20**, 17635-17639; (d) J.-P. Wan, D. Hu, Y. Liu and S. Sheng, *ChemCatChem* 2015, **7**, 901-903; (e) J.-P. Wan, S. Cao and Y. Liu, *Org. Lett.* 2016, **18**, 6034-6037; (f) S. Panda, P. Maity and D. Manna, *Org. Lett.*, 2017, **19**, 1534-1537.
56 Z. Mo, A. Rit, J. Campos, E. L. Kolychev and S. Aldridge, *J. Am. Chem. Soc.*, 2016, **138**, 3306-3309.
57 M. K. Barman, S. Waiba and B. Maji, *Angew. Chem., Int. Ed.*, 2018, **57**, 9126-9130.
58 CCDC 1866759 contains the supplementary crystallographic data for this paper.
59 S. Keess and M. Oestreich, *Chem. Sci.*, 2017, **8**, 4688-4695.
60 Q. Wang, J. Chen, X. Feng and H. Du, *Org. Biomol. Chem.*, 2018, **16**, 1448-1451.
61 T. Mondal, S. Dutta, S. De, D. Thirumalai and D. Koley, *J. Phys. Chem. A,* 2019, **123**, 565-581.
62 S. Dutta, B. Maity, D. Thirumalai and D. Koley, *Inorg. Chem.,* 2018, **57**, 3993-4008.
63 (a) D. Roy and R. B. Sunoj, *Org. Lett.*, 2007, **9**, 4873-4876; (b) k. Ando, *J. Org. Chem.*, 2010, **75**, 8516-8521; (c) R. Sharma, M. Thorley, J. P. McNamara, C. I. F. Watt and N. A. Burton, *Phys. Chem. Chem. Phys.*, 2008, **10**, 2475-2487.
64 Deprotonation from N^4 center will afford highly unstable intermediate (ΔG_L^S = 37.6 kcal mol^{-1}) higher than $\mathbf{17_{bba}}$.
65 L. Greb, S. Tamke and J. Paradies, *Chem. Commun.,* 2014, **50**, 2318-2320.

View Article Online
DOI: 10.1039/C9SC02492A

66 Y. Ma, S. -J. Lou, G. Luo, G. Zhan, M. Nishiura, Y. Luo and Z. Hou, *Angew. Chem., Int. Ed.,* 2018, **57**, 15222-15226.
67 The energy span in *Part IV* ($\mathbf{18}_{aca}\rightarrow\mathbf{20}_{aca}$) is reduced by ca. 4.0 kcal/mol when intermediates for the step $\mathbf{17}_{aca}\rightarrow\mathbf{18}_{aca}$ was optimized in benzene continuum (B3LYP/SVP(CPCM) level).
68 M. J. Frisch, G. W. Trucks, H. B. Schlegel, G. E. Scuseria, M. A. Robb, J. R. Cheeseman, G. Scalmani, V. Barone, B. Mennucci, G. A. Petersson, H. Nakatsuji, M. Caricato, X. Li, H. P. Hratchian, A. F. Izmaylov, J. Bloino, G. Zheng, J. L. Sonnenberg, M. Hada, M. Ehara, K. Toyota, R. Fukuda, J. Hasegawa, M. Ishida, T. Nakajima, Y. Honda, O. Kitao, H. Nakai, T. Vreven, J. A. Montgomery Jr., J. E. Peralta, F. Ogliaro, M. Bearpark, J. J. Heyd, E. Brothers, K. N. Kudin, V. N. Staroverov, T. Keith, R. Kobayashi, J. Normand, K. Raghavachari, A. Rendell, J. C. Burant, S. S. Iyengar, J. Tomasi, M. Cossi, N. Rega, J. M. Millam, M. Klene, J. E. Knox, J. B. Cross, V. Bakken, C. Adamo, J. Jaramillo, R. Gomperts, R. E. Stratmann, O. Yazyev, A. J. Austin, R. Cammi, C. Pomelli, J. W. Ochterski, R. L. Martin, K. Morokuma, V. G. Zakrzewski, G. A. Voth, P. Salvador, J. J. Dannenberg, S. Dapprich, A. D. Daniels, O. Farkas, J. B. Foresman, J. V. Ortiz, J. Cioslowski and D. J. Fox, *Gaussian* 09, *Revision D.01*, Gaussian, Inc., Wallingford CT, 2013.
69 (a) G. te Velde, F. M. Bickelhaupt, E. J. Baerends, C. Fonseca Guerra, S. J. A. van Gisbergen, J. G. Snijders and T. Ziegler, *J. Comput. Chem.,* 2001, **22**, 931–967; (b) GUI 2013, SCM, Amsterdam, The Netherlands, http: //www.scm. com.
70 (a) A. D. Becke, *J. Chem. Phys.*, 1993, **98**, 5648-5652; (b) C. Lee, W. Yang and R. G. Parr, *Phys. Rev. B: Condens., Matter Mater. Phys.,* 1988, **37**, 785-789.
71 A. Schäfer, H. Horn and R. J. Ahlrichs, *J. Chem. Phys.*, 1992, **97**, 2571-2577.
72 T. A. Helgren and W. N. Lipscomb, *Chem. Phys. Lett.*, 1977, **49**, 225-232.
73 S. Grimme, J. Antony, S. Ehrlich and H. A. Krieg, *J. Chem. Phys.*, 2010, **132**, 154104-154122.
74 A. Schafer, C. Huber and R. Ahlrichs, *J. Chem. Phys.*, 1994, **100**, 5829−5835.
75 M. Cossi, G. Scalmani, N. Rega and V. Barone, *J. Comput. Chem.*, 2003, **24**, 669-681.
76 (a) E. D. Glendening, A. E. Reed, J. E. Carpenter and F. Weinhold, NBO Version 3.1; (b) A. E. Reed, L. A. Curtiss and F. Weinhold, *Chem. Rev.*, 1988, **88**, 899–926.
77 R. F. W. Bader, *Chem. Rev.*, 1991, **91**, 893–928.
78 (a) M. Mitoraj and A. Michalak, *Organometallics*, 2007, **26**, 6576–6580; (b) M. P. Mitoraj, A. Michalak and T. Ziegler, *J. Chem. Theory Comput.*, 2009, **5**, 962– 975.
79 (a) K. Morokuma, *J. Chem. Phys.*, 1971, **55**, 1236–1244; (b) K. Kitaura and K. Morokuma, *Int. J. Quantum Chem.*, 1976, **10**, 325–340.
80 (a) T. Ziegler and A. Rauk, *Inorg. Chem.*, 1979, **18**, 1755–1759; (b) T. Ziegler and A. Rauk, *Theor. Chim. Acta*, 1977, **46**, 1–10.
81 T. Mondal, S. Dutta, S. De and D. Koley, *J. Org. Chem.,* 2019, **84**, 257-272.
82 S. Dutta, T. Mondal, S. De, K. Rudra and D. Koley, *Inorg. Chim. Acta,* 2019, **485**, 162-172.
83 G. Frenking, K. Wichmann, N. Fröhlich, C. Loschen, M. Lein, J. Frunzke and V. M. Rayon, *Coord. Chem. Rev.,* 2003, **238**–**239**, 55−82.
84 F. M. Bickelhaupt and K. N. Houk, *Angew. Chem., Int. Ed.,* 2017, **56**, 10070-10086.
85 T. Mondal, S. De and D. Koley, *Inorg. Chem.,* 2017, **56**, 10633-10643.
86 C. Y. Legault, CYLview, 1.0b, Université de Sherbrooke, 2009, See http: //www.cylview.org.

View Article Online
DOI: 10.1039/C9SC02492A

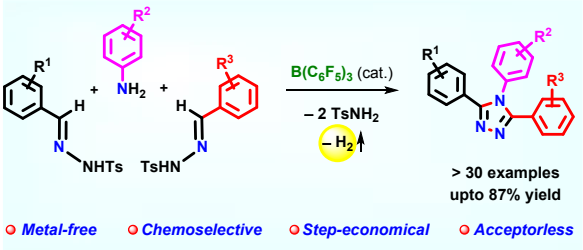

Metal-free acceptorless-dehydrogenative-cyclization of *N*-tosylhydrazones and aromatic amines produces both symmetrical and unsymmetrical 1,2,4-triazoles in high yields and selectivities.